INVESTIGATION OF THE HEATING EFFECT OF MRI ON THE PATIENTS WITH METALLIC ORTHOPAEDIC IMPLANT MATERIALS

By

Mehmet Salih Bilgin

B.S. in Electrical and Electronic Engineering
Boğaziçi University, 1995

Submitted to the Institute of Biomedical Engineering
in partial fulfilment of the Requirements
for the degree of
Master of Science
in
Biomedical Engineering

Boğaziçi University

September, 1999

ACKNOWLEDGEMENTS

Before starting, I like to send my best wishes to my supervisor Ass. Prof. Mehmed Özkan, who gave me the chance to study a very exciting topic, and who was available to help me with his great experience and endless support.

Dr. Mehmet Calay and Dr. Farzın Peirovi, were very kind for giving me a lot of ideas and support during my experiences.

People of, E M A R private MRI practice that we have performed the experiences, were very kind for giving me the opportunity of using their highly sophisticated and expensive equipment.

Also, the doctors of Çapa School of medicine Orthopaedics and traumatologics department were very kind in supplying me a lot of information about the orthopaedic implant materials and lots of valuable information.

Prof. Dr. Özenç Minareci, and Yrd. Doç. Ahmet Ademoğlu were very kind in giving me ideas about how to progress during my studies.

The 'Evrenler' company has manufactured the implant we have used, as a special design. I must thank to them.

AN INVESTIGATION OF THE MRI SEQUENCES ON THE PATIENTS WITH ORTHOPAEDIC IMPLANT MATERIALS

Mehmet Salih Bilgin
Biomedical Engineering, M.S. Thesis, 1999
Thesis Supervisor: Doç. Dr. Mehmed Özkan

Keywords: Orthopaedic Implants, MRI, Eddy Currents.

ABSTRACT

It is increasingly becoming common that orthopaedic patients are having implant materials in their body. On the other hand MRI with its potential diagnostic value can not be utilised well on the patients with metal implants due to potential hazardous interaction of metal and magnetic field. Normally, if a metal is facing a magnetic field change, there is the induction of eddy currents on the metal and the induced currents are being dissipated through the resistance of the metal, producing heat.

The aim of this study is to investigate the temperature rise due to metal implant and MRI interaction. For this purpose we have prepared a phantom, which comprises a metallic implant embedded in polyacrylamide gel in order to simulate the human tissue and the implant material inside.

This phantom is scanned under MRI using the common protocols for the orthopaedic patients. The temperature rise has been monitored during the scanning. A theoretical model of the heat dissipation has been established.

Eddy current induction on metals is due to the change of magnetic field applied on the metal planes. There are two sources of magnetic field in MRI, the gradient field and the RF field. It has been observed that there is a temperature rise due to the gradient fields and the RF system of the MRI equipment. As a result of this study we showed that using present MR technology the amount of the temperature rise observed remains within the tolerable range not to cause tissue necrosis when the implant is made of stainless steel metal.

MRG SEKANSLARININ ORTOPEDİK İMPLANT MALZEMELİ HASTALARDAKİ ETKİLERİ

Mehmet Salih Bilgin
Biomedical Engineering, M.S. Thesis, 1999
Thesis Supervisor: Doç. Dr. Mehmed Özkan

Keywords: Orthopaedic Implants, MRI, Eddy Currents.

ÖZET

Günümüzde ortopedi kliniklerinin çoğu hastalarının vücutlarında protezler veya implant malzemeler bulunmakta ve büyük diagnostik potansiyeli olmasına rağmen bu hastalara MRG tetkiki rahatlıkla yapılamamaktadır. Normal olarak bir metalin üzerindeki manyetik alan değişiyor ise, bu metalin üzerinde indüksiyon akımları oluşmaktadır. Oluşan bu akımlar metalin direnci üzerinde ısıya dönüşmektedir.

Bu çalışmanın amacı MRG esnasında bu gibi hastalarda oluşabilecek sıcaklık artışı hakkında bilgi vermektir. Bu amaçla metal implante edilmiş insan vücudunun yerini tutması amacı ile polyacrylamide jel'den oluşan ve içinde metalik implant malzeme bulunan bir fantom yapılmıştır.

Bu fantom genellikle orthopedik hastalara uygulanan MRG protokolleri kullanılarak taranmıştır. Tetkikler sırasında oluşan sıcaklık değişimleri monitörize edilip, teorik olarak ısı dağılımının modellemesi yapılmıştır.

Metal üzerinde indüksiyon akımlarının oluşumu temel olarak manyetik olan değişiminden kaynaklanmakta olup bu değişken manyetik alanın iki kaynağı sistemin Gradient ve RF üniteleridir. MRG sisteminin değişen gradient alanlarından ve RF sisteminden kaynaklanan bir ısı değişimi gözlenmiştir. Bu çalışmanın sonucunda şu anda kullanılmakta olan MR sistemlerinde stainless-steel metal implant malzemeli hastalarda oluşan ısı artışının çevre dokularda herhangi bir doku nekrozu'na sebebiyet vermeyecek boyutta olduğu saptanmıştır.

TABLE OF CONTENTS

LIST OF FIGURES

LIST OF TABLES

LIST OF SYMBOLS

B_0	Magnetic Field
c	Specific Heat
D	Distance Between Gradient Coils
dV	Volume Element
dB/dt	Magnetic field Change Rate
E	Electric Field
GE	Gradient Echo (Field Echo)
J	Current Field
m	Mass
M	Magnetisation Vector
M_L	Longitudinal Component of the Magnetisation Vector
M_T	Transverse Component of the Magnetisation Vector
MRA	MR Angio
P	Instantaneous power
PD	Proton Density
R, r	Radius of the implant
S	Signal Intensity
SE	Spin Echo
SR	Slew Rate
T1	Longitudinal Relaxation time
T2	Transverse Relaxation time
TE	Echo time
TR	Repetition time
ΔT	Change of temperature
γ	Gyromagnetic Ratio
ρ	Resistivity
σ	Permittivity
w_0	Precessional Frequency

1. INTRODUCTION

Medicine is one of the fields that change rapidly with the technological improvements. The fields of Radiology and Orthopaedics have been affected from the technological improvements, too. The most exciting development in diagnostic imaging in recent years has been the application of nuclear magnetic resonance (NMR) techniques in diagnostic imaging and creating a new imaging modality called Magnetic Resonance Imaging (MRI) [1]. Basically, MRI makes use of magnetic fields and radiofrequency (RF) waves to generate intensity-modulated images from specific sections of the body. The intensity of a point within an image is determined in a complicated way by the number of hydrogen atoms at the corresponding point in the patient and also the chemical makeup of the tissue at that point. Signal intensity is measured by placing the patient in a strong magnetic field, irradiating the region of interest with RF waves, and recording the radiation re-emitted from the patient. Resolution of MRI images are, so useful that it is the best way of showing the soft tissue contrast for diagnostic imaging.

In orthopaedics advances in material science and surgery techniques allow the replacement of the joints and bones with implant materials, such as metals, Iron-based alloys, Cobalt-based alloys, Titanium and Titanium-based alloys, Polymers and Ceramics [2]. For optimal performance in physiologic environments, implant materials should have suitable mechanical strength, biocompatibility, and structural biostability [3].

MRI is the second most frequently used and requested diagnostic tool after direct radiographic diagnosis, for an orthopaedics clinic [4]. However, a great deal of the patients of such a clinic has implanted prosthesis inside of their body. Because of the safety concerns these patients are not admitted into MRI scanner, as a precaution.

The U.S. FDA (United States Food and Drug Administration) requires labelling of MRI scanners to indicate that the device is hazardous for patients who have electrically, magnetically, or mechanically activated implants, because the magnetic and electromagnetic fields produced by the MRI device may interfere with the operation of these devices.

Therefore, patients with internal cardiac pacemakers, implantable cardiac defibrillators, cochlear implants, neurostimulators, bone-growth stimulators, implantable drug infusion pumps, and other similar devices that could be adversely affected by the electromagnetic fields used for MRI should not be examined by this imaging modality [5]. The associated risks of scanning patients with cardiac pacemakers are related to the possibility of movement, reed switch closure or damage, programming changes, inhibition or reversion to an asynchronous mode of operation, electromagnetic interference, and induced currents in lead wires. One particular concern may be the possibility of one lead wire could easily act as an antenna in which the gradient and / or RF electromagnetic fields may induce sufficient current to cause fibrillation, a burn, or other potentially dangerous event. In the case of similar implants the situation is not so different than that of the cardiac pacemakers.

For an orthopaedics clinic the implanted materials to the patients are mostly the metals, such as titanium and stainless steel. Although there is a wide range of orthopaedic implant materials, we have investigated the induced currents and their heating effects on the metal implants, and particularly we have focused on stainless steel due to its common use. The potential risks associated with performing MRI to patients with ferromagnetic implant materials, or devices are related to:

(a) the induction of electrical currents;

(b) heating;

(c) the misinterpretation of an artefact as an abnormality;

(d) the possibility of movement or dislodgement [5].

In this study we have investigated the heating effect due to induced eddy currents. The finding, is aimed to be utilised during the decision of applying MRI to the patients with metallic implant materials.

Chapter 1 is a brief outline about the effects of MRI on some implanted devices. In chapter 2 some background on the orthopaedic implant materials is presented. Chapter 3 is a summary of Magnetic Resonance Imaging. In this chapter interaction between MRI and implants is also introduced. In Chapter 4 the experimental set up, experiments and the

phantom formation has been described. Chapter 5 is the discussions of the experimental results and includes conclusions. In Chapter 6 discussions about the results have been presented.

2. IMPLANT MATERIALS INSIDE HUMAN BODY

The implant materials are those used for fixation purposes for supporting the osseointegration process and they are slightly different than the prosthesis materials which are mostly used to replace a joint or even to replace the function of an obsolete bone. In this study we have focused on the stainless steel type of metallic implant materials since they are having more ferromagnetic material content, as they would have more heating effect [4] as compared to the proateases, which are mostly an alloy of titanium [6].

Biologic classification of implant materials is based on tissue response and on the systemic toxicity effects of the implant. There are three classes of biomaterials: biotolerant, bioinert, and bioactive. Biotolerant materials such as, stainless steel and PMMA (polymethylmethacrylate), are usually binded by a thin fibrous tissue layer at the bone-implant interface. The fibrous tissue layer develops as a result of irritation of the surrounding tissue through leaching processes [6]. Bioinert materials such as cobalt alloys, titanium, and aluminum oxide, are characterised by direct bone contact, or osseointegration, at the interface under favourable mechanical conditions. Osseointegration is achieved because the material surface is chemically nonreactive to the surrounding tissues and body fluids. Finally, bioactive materials, such as bioglass and calcium phosphate ceramics, have a bone-implant interface characterised by direct chemical bonding of the implant with surrounding bone. This chemical bond is caused by the presence of free calcium and phosphate compounds at the implant surface [6].

The most commonly used biomaterial combinations for orthopaedic implants are metals and their alloys articulating with ultrahigh molecular weight polyethylene (UHMWPE). For example, stainless steel is an iron-based alloy and is mostly used as hip prosthesis and is the material of choice for internal fixation plates, rods, and screws. Developments in materials science have produced stronger cobalt- and titanium- based alloys. The wear resistance of cobalt-based alloys makes them desirable for applications involving articulating surfaces. Titanium-based alloys are having the closest modulus of elasticity to that of a bone than other

metal materials and they are being manufactured as femoral stems to reduce the effects of stress shielding [6].

Polymers and ceramics are also important classes of materials for orthopaedic implant applications. UHMWPE has a very low coefficient of friction and it is ideal for an articulating surface with metals. PMMA has been used as a grouting agent in total joint arthroplasty. Aluminum oxide has gained popularity as a ceramic femoral head due to its high wear resistance and low coefficient of friction. Finally, calcium phosphate ceramics, particularly hydroxyapatite (HA), have been used in monolithic form as an augmentation material for metaphyseal bone defects and as a coating on metal devices for total joint arthroplasty [6].

Every type of implant material has valuable applications in the field of orthopaedics, but since we are only dealing with the heat effect and the eddy current phenomenon on the metals, we will only deal with metal implant materials in this study.

The suitability of a metal component for maintaining longevity of a total joint replacement depends on the design of the implant and the biocompatibility, strength, wear and corrosion characteristics of the metal. The most important characteristics are yield strength, ultimate tensile strength, and fatigue strength. These parameters can be determined from stress-strain and fatigue limit curves. The composition specifications and mechanical characteristics of all metals and their alloys used for orthopaedic implants have been standardised by the American Society for Testing and Materials (ASTM) [6].

The metal implant materials can be classified in to three major categories according to their base materials. Namely, the iron, cobalt and titanium are the three major base materials of the metallic implants [6].

Iron based alloys or the so-called stainless steels are further divided into subgroups according to their microstructure. For example the austenitic or the group III stainless steels are used for orthopaedic implants [6]. These stainless steel materials are mostly referred with their codes 316 and 316L. The basic difference between the two is their carbon content. The ASTM specifications for the chemical composition of these two metals are summarised in Table1. The resistivity of the 316L stainless steel is 0.75 Ω mm^2 / m and the thermal

conductivity of the same material is 15.0 W/ m K. The reasons for choosing 316L stainless steel in our experiments are presented in part 4.2.

Table 1
Chemical composition of stainless steel materials

	Maximum Amount (%)	Maximum Amount (%)
Element	316	316L
Carbon	0.08	0.030
Manganese	2.00	2.00
Phosphorus	0.030	0.030
Sulfur	0.030	0.030
Silicon	0.75	0.75
Chromium	17.00 to 19.00	17.00 to 19.00
Nickel	12.00 to 14.00	12.00 to 14.00
Molybdenum	2.00 to 3.00	2.00 to 3.00
Nitrogen	0.10	0.10
Copper	0.50	0.50
Iron	Balance	Balance

Molybdenum is added to the stainless steel alloys to increase resistance against corrosion. They are most appropriate for temporary devices such as bone plates, bone screws, hip nails, and intramedullary nails. Also, doping with molybdenum is preferred with cobalt-based alloys.

Second important class of metal alloys is the cobalt-based alloys. The ASTM specifications for the chemical composition of cobalt-based alloys are summarised in Table 2. Electrical and thermal properties are similar to those of stainless steel. The basic difference

between the cobalt-based alloys and the stainless steel is that cobalt-based alloys have slightly higher electrolytic coefficients as compared to the stainless steel. So the cobalt-based alloys' long-term performance inside the body is a little bit worse than that of the stainless steel, in the sense that they cause more electrical potential inside the body when they react with the saline environment of the human body.

Table 2
Chemical composition of cobalt-based alloy materials

	Maximum Amount (%)	Maximum Amount (%)
Element	Cast Co-Cr-Mo	Wrought Co-Ni-Cr-Mo
Carbon	0.35	0.025
Manganese	1.00	0.15
Phosphorus	-	0.015
Sulfur	-	0.010
Silicon	1.00	0.15
Chromium	30.00	21.0
Nickel	1.00	37.0
Molybdenum	7.00	10.5
Titanium	-	1.00
Iron	0.75	1.00
Cobalt	Balance	Balance

Cobalt-based alloys have mechanical properties suitable for load bearing implant applications. These alloys are characterised by high fatigue and ultimate tensile strength that make them appropriate for applications requiring long service life without fracture. The high

wear resistance of these alloys also makes them desirable for load bearing and for using at articulating surfaces.

Titanium and titanium-based alloys are also important types of implant metals. Commercially pure titanium and titanium-based alloys are low-density metals that have chemical properties suitable for implant applications. The ASTM specifications are summarised in Table 3.

Table 3
Chemical composition of Titanium and Titanium alloy materials.

	Maximum Amount (%)	Maximum Amount (%)	Maximum Amount (%)
Element	Unalloyed Titanium	Wrought Ti6Al4V ELI Alloy	Cast Ti6Al4V Alloy
Carbon	0.10	0.08	0.05
Nitrogen	0.05	0.05	0.05
Hydrogen	0.015	0.012	0.015
Oxygen	0.40	0.13	0.20
Aluminum	-	5.5 to 6.5	5.5 to 6.75
Vanadium	-	3.5 to 4.5	3.5 to 4.5
Iron	0.50	0.25	0.20
Titanium	Balance	Balance	Balance

The strength of titanium and titanium-based alloys are almost half of the other metals but it is at least five times greater than that of a bone. This group is mostly used for replacement purposes, rather than fixation purposes. They have the lowest electrolytic coefficients as compared to the former two groups but they don't have good performance when combined with the cement used for fixation purposes.

3. MAGNETIC RESONANCE IMAGING

The basic imaging principles of MRI is particularly important for us to comprehend the reasons of temperature change or the energy transfer on to the materials that are undergoing MRI examination.

Basically, MRI makes use of magnetic fields and radiofrequency (RF) waves to generate intensity-modulated images from specific sections of the body. The intensity of a point within an image is determined in a complicated fashion by the number of hydrogen protons at the corresponding point in the patient and also the chemical makeup of the tissue at that point. Signal intensity is measured by placing the patient in a strong magnetic field, irradiating the region of interest with RF waves, and recording the radiation reemitted from the patient [7].

3.1 Physical Principles of MRI

The principle of Nuclear Magnetic Resonance (NMR) is based on the fact that certain nuclei have an odd number of neutrons or protons, creating a charge distribution that results in each nucleus possessing a characteristic called spin angular momentum, and thus a magnetic moment. This concept can be illustrated by considering the nucleus to resemble a small spinning top as shown in Figure 1 [7]. Since the nucleus has a positive charge and is in motion, it becomes a magnetic dipole and generates a magnetic field similar to that of a small bar magnet. The magnetic field is characterised by the magnetic moment, which is a vector quantity because the magnetic field has both a specific strength and direction. There are many atoms whose nuclei exhibit spin and therefore have magnetic moment (i.e. ^{1}H, ^{13}C, ^{19}F, ^{23}Na, ^{31}P, and ^{39}K). Since hydrogen atoms constitute a vast majority of the atoms in the human body, this abundance makes in vivo proton (^{1}H) MRI possible.

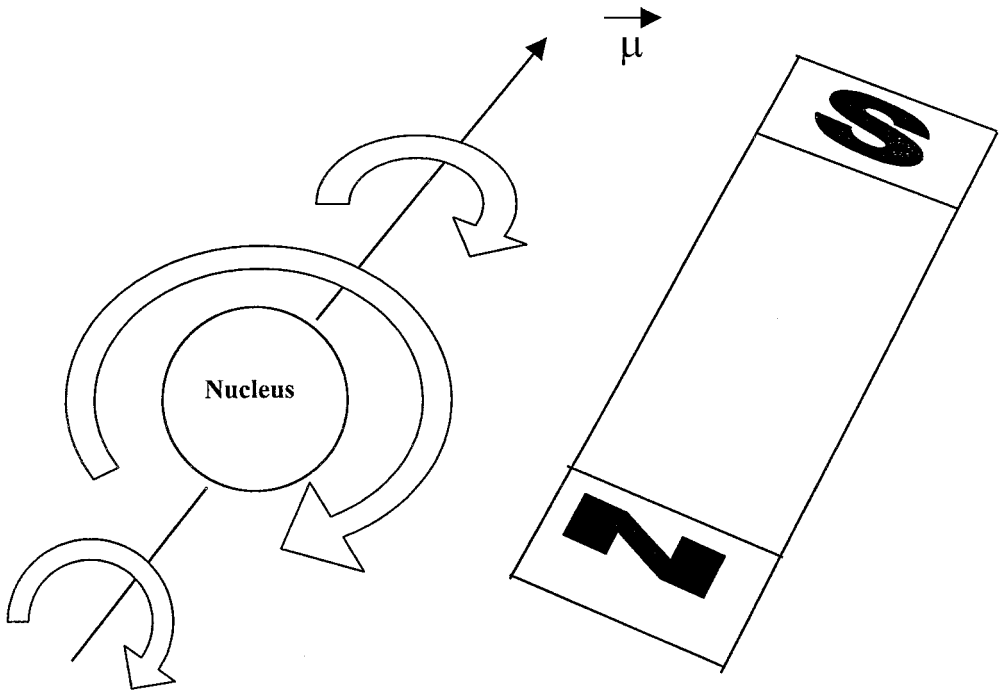

Figure 1 A nucleus with an odd number of neutrons or protons possesses spin angular momentum and thus generates a magnetic field, like a bar magnet with a magnetic moment μ pointing in the direction of the magnetic and functionally with a north pole (N) and a south pole (S) [7].

When no magnetic field is present, the nuclei in the region of interest are oriented at random positions. However, when placed in a static magnetic field (B_0), the nuclei experience a torque that causes a majority of them to align with the magnetic field direction. As the nuclei align themselves, they begin to oscillate or precess about the direction of the applied magnetic field. This motion is very similar to the wobbling of a spinning top that is trying to maintain its alignment with the gravitational field of the earth [7].

The frequency at which the nuclei precess is different for different nuclei, but is the same for identical nuclei and is directly proportional to the strength of the applied magnetic field. This precessional frequency is called the Larmor frequency and is the fundamental basis for NMR [7]. For the magnetic field strengths used in imaging (0.05 to 2.0 tesla), this frequency falls in the RF band. The Larmor equation:

$$w_0 = \gamma B_0 \qquad (1)$$

provides the relationship between the precessional frequency, w_0 , and the applied static magnetic field strength, B_0 . The proportionality constant, γ , is called the gyromagnetic ratio and is unique for each type of nucleus [8]. For example, for hydrogen nuclei γ is approximately 42.58 mHz/T.

In general, the application of a magnetic field to a quantity of identical nuclei makes them to be directed in the direction of the magnetic field (some are anti-parallel but a majority parallel to the field) and their precession about that direction. These nuclei all precess at the Larmor frequency but with random phase. However, since their individual magnetic moments are tending toward the direction of the applied magnetic field, the individual moments sum together by vector addition to produce a net magnetisation or net magnetic moment, along the direction of the applied magnetic field. The magnitude of the net magnetic moment is determined by the number of hydrogen nuclei present and also by the strength of the static magnetic field. There is no net precession of the net magnetic moment around its direction because the phases of the individual magnetic moments are randomly distributed and therefore their components in the horizontal plane cancel each other. Thus no signal can be detected from the precession of the nuclei in this equilibrium orientation.

To cause the nuclei to generate a detectable NMR signal, it is necessary to change the orientation of the net magnetic moment. This is accomplished by the application of external energy so that net magnetic moment is no longer parallel to the static magnetic field. This external energy is applied by an RF pulse emitted from a coil that serves as a transmitting antenna. This pulse varies with time and is perpendicular to the direction of the static magnetic field. For energy to be absorbed so that the net magnetic moment can be tilted away from the direction of the static magnetic field, the frequency must exactly match the resonant frequency (Larmor frequency) of the nuclei. The effect of this coherence is that the individual magnetic moments begin to align themselves to each other and precess in phase. When the RF pulse is turned on, the net magnetic moment then begins to tilt from the direction of the static magnetic field as shown in Figure 2 [8]. It will then have two components, a longitudinal or parallel component, (M_L), and a transverse or perpendicular component, (M_T). If the pulse is left on

long enough, the net magnetic moment will be rotated 90^0 and lie in the transverse plane (plane x-y perpendicular to the static magnetic field). Thus in the transverse plane M_L=0 and M_T=M. Since the net magnetic moment has been rotated (flipped) 90^0 the applied pulse is therefore called a 90^0 pulse. At the instant the RF pulse is turned off, all the individual nuclei are precessing in phase so that the net magnetic moment is precessing about the static magnetic field in the x-y plane. The nuclei immediately begin to dephase because of localised differences in the magnetic field due to molecular environments, and the net magnetic moment begins to return to its previous state parallel to the applied static field because of the tendency of nuclei to align themselves with the field. This moving magnetic moment can induce a voltage in a receiver coil (also perpendicular to the static magnetic field) that varies with the same frequency as the applied field and decays with time as the net magnetic moment returns to its original state. This phenomenon of relaxation is called free-induction decay and its magnitude decreases exponentially with time [9]. The initial amplitude of this signal is proportional to the number of hydrogen nuclei present in the sample and therefore is a measure of proton density. M_L and M_T can be plotted as a function of time as M returns to its original state and yields exponential growth and decay curves respectively as shown in Figures 3 and 4 [8].

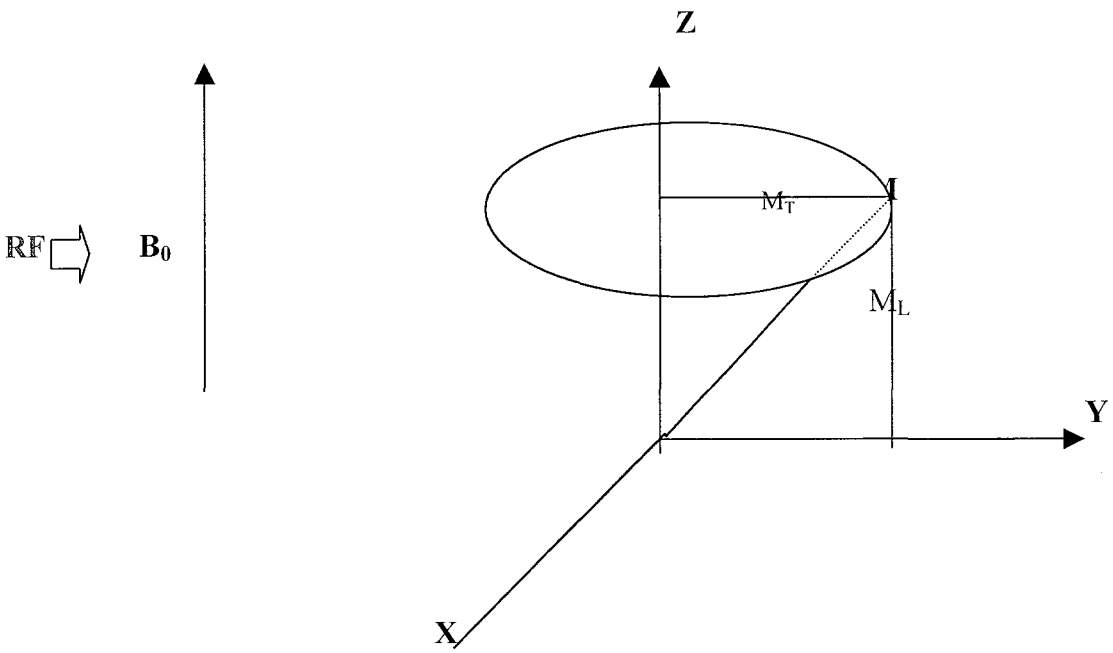

Figure 2 Application of RF energy perpendicular to the net magnetic moment M causes M to spiral away from the direction of the applied field, B_0. M will then have a longitudinal (M_L) and a transverse (M_T) component.

The equations for these two curves as a function of time (t) are given by:

$$M_L = M (i - e^{-t/T1}) \quad (2)$$

$$M_T = M e^{t/T2} \quad (3)$$

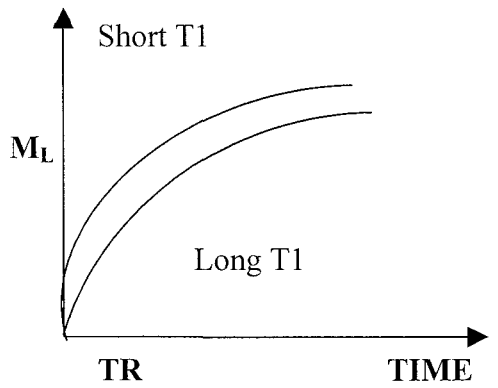

Figure 3 Plot of the longitudinal (M_L) component of M as it returns from transverse plane to a position parallel to the applied field.

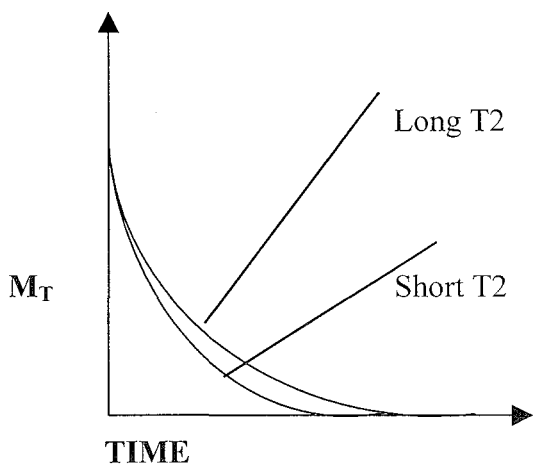

Figure 4 Plot of the transverse (M_T) component of M as it returns from transverse plane to a position parallel to the applied field.

The variables T1 and T2 mathematically are time constants and are generally called relaxation times. T1 is the time required for M_L to recover to 63% of the magnitude of M. It is called the spin lattice or longitudinal relaxation time and is affected by the molecular composition of the environment in which the hydrogen nuclei is belonging. T2 is the time

required for $\mathbf{M_T}$ to fall to 37% of the magnitude of M. It is called the spin-spin or transverse relaxation time and is affected by slight changes in the magnetic field due to the presence of neighbouring nuclei. Since water is a major component of biological systems, it is the measurement of T1, T2, and proton density of hydrogen nuclei that yield MR images of tissues whose contrast is determined by their chemical structures [8]. Different tissue types (both normal and abnormal) differ in T1 and T2 contrast. Imaging techniques are utilising these differences and determining the diagnostic capabilities of MRI.

Physics of MRI is a very complicated subject. Important parts of the MRI physics for our study are the gradient fields and the RF system. Gradient fields are changing the magnetic field's direction and magnitude, and causing the induction of eddy currents on the metals that are inside of the magnet.

Also, the application of RF field is transferring some energy on the objects under examination. This contribution of RF energy transfer to the imaging volume in the MRI scan is very important. Since the RF system emits RF waves, which are alternating electromagnetic waves, they are the sources of eddy current production on the metals inside the MRI system.

3.2 Imaging Principles

In the previous section we have mentioned that under the existence of a static magnetic field, using a RF pulse we can receive a signal from a group of hydrogen nuclei. The signal's amplitude and the relaxation times depend on tissue characteristics. However, we did not try to determine the spatial locations from which the NMR signal is originated.

In practice, the position is determined by using gradient coils, to linearly change the magnetic field in one or more directions. Since the larmor frequency is determined by the strength of magnetic field, establishment of field gradients causes the resonant frequency to be different for each location within the field. To image a plane, gradients are established to select the plane and to separate individual points within the plane (this is the selection of the slices in practical usage of MRI). RF pulses are applied and a complex series of frequencies are received. The individual frequencies, phases, and amplitudes are then determined using the mathematical techniques of Fourier analysis.

The details of the imaging procedures are beyond the scope of this study and can be found in detail elsewhere [7,8,9]. The three gradient coils corresponding to the X, Y, and Z orthogonal directions that can alter the magnetic field linearly in those directions, images of individual transverse, sagittal, and coronal planes within the body can be obtained. These changes in the magnetic fields are capable of forming eddy currents on the metals facing this field change. These induced eddy currents can result in temperature change on the surrounding tissues.

To form an image RF and gradient fields are excited in certain sequence and each such sequence is called an MRI sequence or protocol.

There are two important and most frequently used pulse sequences in imaging; 1) the spin echo technique, and 2) the field echo (or the gradient echo) technique. The spin echo and field echo techniques have some other newly developed versions called fast or turbo sequences. For the spin echo there is the latest technique called fast advanced spin echo [7].

Let us have a brief look at the spin echo technique. Our aim here is not to get into the details of the sequence but to give an idea about the imaging parameters TE and TR, since their ratio is needed for us in energy transfer calculations. Before starting we can illustrate the pulse shapes that are being used in this technique as in the Figure 5.

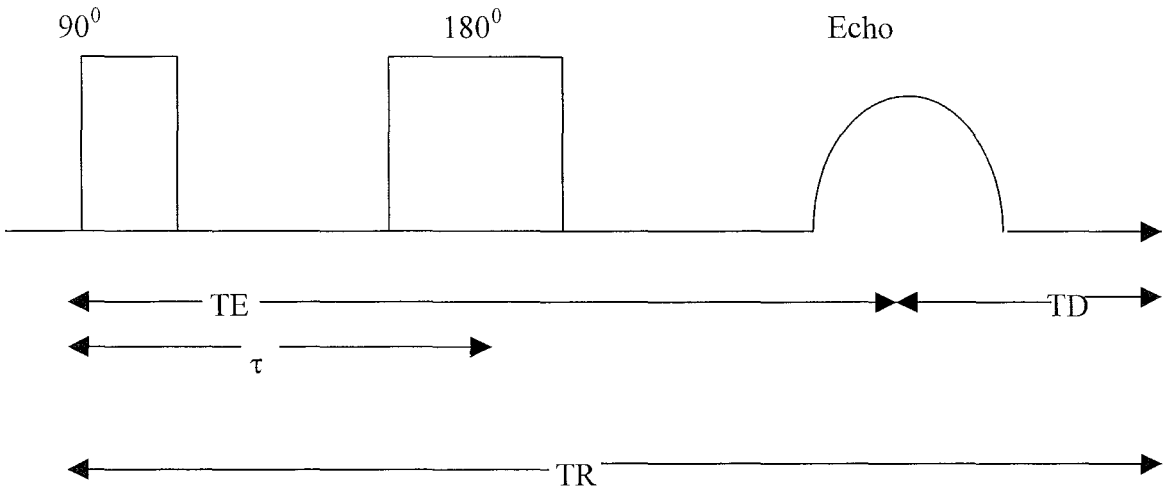

Figure 5 Spin echo pulse sequences uses the combinations of 90^0 and 180^0 pulses, which are the emitted RF pulses and the echo is again the RF pulse to be received.

This technique begins with the application of a 90^0 pulse to move the net magnetic moment into the transverse or X-Y plane. The gradient fields are the turned off letting the magnetic moment to turn to its original position. When the net magnetic moment begins to return to its original position, individual nuclei immediately begin to dephase due to localised differences in magnetic field strength, and the signal from free induction decay appears and fades away. However, the RF receiver is not turned on during this process. Instead after a time τ, a 180^0 is applied to flip the individual magnetic moments, providing a mirror image using the Y-Z plane as the mirror. As the individual moments come back into phase, after a certain time after the application of the 180^0 pulse, an NMR signal (echo) is generated which then disappears as the individual nuclei once again dephase. This echo is "read out" by the receiver coil and used for imaging purposes. The equation that describes the image brightness or MRI signal intensity at a point in an image using the spin echo technique is given by:

$$S = D\,(1 - e^{-TD\,/\,T1})\,e^{-TE\,/\,T2} \qquad (4)$$

Where D is a function of proton density, and T1 and T2 the NMR relaxation times. The delay time, TD, is the time after the signal (echo) is received before the sequence is repeated, and the repetition time, TR, is the total time for a single pulse sequence (sequence interval). Note that the echo time, TE, the time between the 90^0 pulse and the echo, is equal to 2τ where τ is the time between the 90^0 and 180^0 pulses (also the time between the 180^0 pulse and the signal (echo) received in the receiver coil). The parameters TE and TD (or TR) can be set in the data collection process to control the amount of T1 and T2 contribution to the images and to enhance the difference in T1 and T2 [7].

Spin echo is one of the two major groups of pulse sequences in MR imaging. There are also the derivations from this basic spin echo sequences, namely the inversion recovery, fast (turbo) spin echo, fast advanced spin echo etc... these are all based on the idea of flipping the net magnetisation vector to an angle of 90^0 and picking up echoes during its relaxation. The differences between other spin echo families are basically in the order of application of the 180^0 pulse and the number of application of this pulse during one cycle.

Other major group of pulse sequences are called field echo and the major difference is the flip angle of the net magnetisation vector is smaller than 90^0 and the typical value of the flip angle is 20^0. Because of the smaller flip angle the time of acquisition of data is shorter but the soft tissue contrast is lower. But in flow related applications like MRA, (Magnetic Resonance Angiogram) where the speed is important, this group has prime importance.

3.2.1 Imaging types

In general MR images have contributions from three NMR parameters: proton density, T1 and T2. Each of the three parameters may be selectively emphasised in a specific region through the appropriate selection of the combinations of 90^0 and 180^0 RF pulses and gradient values, all in a predetermined time sequence. Proper pulse sequence selection in MR imaging is the key factor of obtaining high quality diagnostic information.

Parameters like the duration of an imaging cycle (TR) is normally a choice of the operator and the echo is acquired TE seconds after the RF pulse. When a short TR is used to obtain a T1 weighted image, the longitudinal magnetisation does not have the opportunity to

approach its maximum and produce high signal intensity. In this case some signal strength must be sacrificed to gain a specific type of image contrast. Also, when TR is reduced to decrease image acquisition time, image noise often becomes a limiting factor. Where relatively, long TE values allow the transverse magnetisation and the signal it produces to decay to very low values.

A proton density weighted image is the one in which the brightness of each tissue is determined by the density, or concentration, of active protons. Both, fat and non-moving fluids have relatively high proton concentrations. Grey matter has a higher proton concentration than white matter and therefore appears brighter in a proton density weighted image. Such an image is obtained by, selecting TR and TE values that minimise the effects of tissue T1 and T2 on image brightness and contrast. A relatively long TR value allows all tissue to reach their maximum longitudinal magnetisation, which is proportional to proton density. This condition is reached when TR is approximately three times longer than the T1 values of the tissue. Proton density images also require short TE. The ideal value would be a TE of 0, but, for most systems, the minimum TE value is in the range of 15 to 30 msec.

In forming an image, the RF pulses must be applied repetitively. After each pulse the magnetisation of the sample is either reduced or is equal to zero. Rapid repetition would not allow much magnetisation to be re-established, and little signal would be seen. Thus, a certain time interval, TR is introduced between successive RF pulses. As the interval TR increases, the signal increases, but so does the imaging time.

In a T1 weighted image, the contrast between tissues is determined by their T1 values. The tissue with a shorter T1 value appears brighter. This is because they regain their longitudinal magnetisation faster than the tissues with the longer T1 values.

A T1 weighted image is obtained by selecting a relatively short TR value. T1 contrast is developed during the early re-growth of longitudinal magnetisation. Therefore, relatively short TR value is required in order to acquire the image when T1 contrast is high. Good T1 contrast is obtained when the TR is approximately equal to the T1 values of the tissue. A short TE is used to minimise contributions from the T2 characteristics of the tissue.

After exposure to an RF pulse, the signal emitted by a sample of proton decays as local inhomogenities of the magnetic field cause the resonance of protons within the sample to lose synchronisation. The amount of signal available decays exponentially in time, with a time

constant characterised by T2, or the "spin-spin" relaxation time, which reflects magnetic interactions between protons. The interval between the application of an RF pulse and reception of a signal (a spin echo) is given by a parameter called TE. As TE increases, the amplitude of the signal decreases and contrast between tissues with different value also changes.

Tissue brightness and contrast in a T2 weighted image are determined by the T2 values of the tissue. In this case, tissue with the longer T2 appears brighter. This is because these tissues maintain their transverse magnetisation longer than the tissues with shorter T2 values. This is essentially the reversal of the development of the T1 contrast. In a T2 weighted image, fluids having long T2 values are often the brightest.

T2 weighted images are obtained by using a combination of long TR and TE values. The long TR eliminates the T1 effects. The long TE allows T2 contrast adequate time to develop during the decay of the transverse magnetisation. It is not possible with conventional imaging procedures, to produce an image with contrast limited to one tissue characteristic. There is always some contribution from at least from one of the other factors. The general objective is to select TR and TE values that will minimise this contribution and produce maximum contrast for the tissues of interest.

3.3 RF Coils and RF System

RF coils of the MRI system are the transmitters and/or receivers of the RF signal to and/or from the patient.

In an MRI system, in order to form an image we basically need three things. One is of course a static magnetic field, other is gradient fields and the RF fields. To form an image, RF and gradient fields are excited in sequence and each certain sequence is referred as an MRI sequence or protocol.

As one can understand from the name, RF system is emitting and receiving RF signals to the object under examination. Since RF signals are electromagnetic fields, they have certain amount of energy, which can easily be transferred to the objects under examination.

Furthermore, these fields may induce eddy currents on the metallic materials and these currents will result in heating of the surrounding tissues.

There are various types of RF coils designed for different purposes [7]. Some of them can be receive only or transmit only and some of them can be both transmitter and receiver. Also the basic differences are in the area of interest, such as, body, spine, breast, shoulder, cervical spine, knee, extremities.

The most recent development in the RF coil technology is the development of array coils. Basically, the concept of the array coils is the combination of more than one coils in parallel or in series connection in order to improve the existing S/N ratio by the factor of square root two.

3.4 Heating Effects

Electrical currents can be generated in conductive materials, either by an alternating magnetic field or by movement of conductive materials through the static magnetic field.

During the imaging sequences, the magnetic field and RF pulses are applied several times. Gradient fields are turned on and off with certain high frequency components. Because of the alternating magnetic fields and pulses there is a certain amount of energy induced on the objects that are under examination. Therefore, if there is a patient that has implanted material inside his or her body, this material also faces similar energy transfer. Moreover the induced energy can be in the form of eddy currents if the object is a metal. The induced current is dissipated on the implant and the surrounding tissue in the form of heat. Thus leading to temperature increase on the surrounding tissue. Because of many reasons like the heating effect due to induced currents or magnetisation effect (for permeable metal implants) of the MRI systems there is a concern for sending a patient with implanted material inside to MR scanner for certain diagnostic needs. An Orthopaedist or a Radiologist cannot be sure about the end results of examining the patient under MRI system, by considering the possibility of harming the neighbouring tissues of the implant. Several important factors influence the relative risk of using MRI for patients with ferromagnetic implants or materials. We can state some of these factors as follows:

a) The rate of change of the gradient magnetic field (typical values for MR scanner of today is between 15mT/m/sec and 50mT/m/sec);
b) Specific heat and thermal conductance of the implant material;
c) Geometry of the implant material;
d) Duration of the time it has been in place.

These factors should be carefully considered before subjecting a patient with a ferromagnetic implant to MRI.

As it has been seen in the above paragraphs that the principle of MRI depends on a static magnetic field, the gradient fields and the RF pulses. Everything included in the MRI equipment is related to the production and control of these fields.

The function of the gradient system is basically to change the magnetic field orientation by applying gradient pulses along the directions of X, Y and Z. So these changes in the magnetic field of the MRI system can induce eddy currents on the metals in the field. Therefore, implanted metal materials inside the body, under MRI examination, can be modelled as a conductor under alternating magnetic field, to explain the eddy current phenomenon.

Heating of the implant in our case is due to the dissipation of the induced eddy currents on the implant. The source of the induced eddy currents is the alternating magnetic fields, which are arising from both the RF system and the gradient system. Here we will calculate the current due to gradient system. Later in Chapter 5 we will try to estimate the magnitude of the total eddy currents (i.e. both from RF and Gradients) by utilising our measurements.

In order to calculate the current on the conductor we will use the maxwell equations as follows:

$$- dB/dt = \nabla \times E \qquad (5)$$

Where B is the magnetic field vector, E is the induced electric field vector. Cross product of the ∇ operator and electric field is the curl of the electric field, which is equal to the rate of change of the magnetic field. The rate of change of magnetic field is constant, for MRI systems.

Solving for E gives the below result:

$$E = \tfrac{1}{2}\, r \times dB/dt \quad (6)$$

$$J = \sigma/2\, r \times dB/dt \quad (7)$$

Where, r is the position vector. J is the current density and σ is the permittivity of the metal.

For our MRI system, we have a slew rate (SR) parameter for the gradient field. Slew rate for our case is SR= 28 T/ m / s. Which means in one second and through 1 meter distance the magnetic field becomes 28 T, which is a very high and impossible to obtain field. Here, we need the rate of change of magnetic field. Actually, the gradients are being applied through the distance between the two poles of the gradient coil. So, for our case:

$$dB/dt = SR^{*} D \quad (8)$$

Where D is the distance between poles of the gradient coils, and for our system it is equal to 0,80 meter.

Therefore the rate of change of our magnetic field is: 22.4 T/s.

To calculate the temperature change on the metal, we need to know the duration of the pulse sequences and the power dissipated on the implant. Our implant material is a cylinder, through which the magnetic field is passing through the axis of symmetry. Also, our cylinder is having a radius of 4 mm and length of 128 mm. Since the power is given by the below equation:

$$P = \int \rho\, J^2\, dV \quad (9)$$

The result of the integral from the centre of the cylinder to the surface, will give the following result:

$$P = (\sigma\, h\, \pi / 8)\, |dB/dt|^2\, R^4 \quad (10)$$

Where R is the radius of the cylinder, h is the length of the cylinder.

If we calculate for the values of our system by assuming the worst case (the field is applied to the metal with right angle) where; $\sigma = 1.6\ 10^7\ (\Omega.m)^{-1}$, h = 128 mm, $|dB/dt| = 22.4$ T / s, R = 4 mm. Power is calculated as 0.033 W.

Since the parameters affecting the power are the parameters of our system, this value is same for all sequences.

The total heat energy dissipated on the metal is the power times the duration of the power application.

$$\text{Energy} = P * \Delta t \tag{11}$$

Where Δt, is the time of power application. For any MRI system gradients are turned off during the echo time (TE) and they are turned on for the remaining parts of the pulse repetition time (TR). So, for any sequence Δt is given by the following equation:

$$\Delta t = \text{Scan time} * (1 - (TE/TR)) \tag{12}$$

Finally, the amount of temperature change is calculated from the Thermodynamics. Namely:

$$\text{Energy (cal)} = m\ c\ \Delta T \tag{13}$$

Where m is the mass and c is the specific heat of the implant material. And the numerical values are m=45 g and c = 0.14 cal / g.^{0}C.

As an illustration, if we substitute the parameters of coronal T1 weighted Spin Echo2 sequence in to equation 13, the total energy will become:

$$\text{Energy} = 0.033 * 236 * (1 - 20/300) = 7.27 \text{ Joule.}$$

$$\text{Energy} = 7.27 / 4.18 = 1.74 \text{ cal.} = m\ c\ \Delta T$$

The amount of temperature change of the implant is calculated to be;

$$\Delta T = 1.74 / (45 * 0.14) = 0.28\ ^{0}C$$

This result means that if there were only gradient effect the temperature of the implant would have been risen from 16^{0} C to 16.28^{0} C.

In table 4 the calculated temperature rise for the metal assuming only gradient effect is presented for our MRI sequences which are presented in figure 6 in detail.

Table 4
Calculated temperature rise on the metal for each MRI protocol
for highest expected temperature rise.

Name of the MRI protocol	Calculated temperature rise (^{0}C)
SE1 T1	0.36
SE2 T1	0.28
FSE T2	0.12
GE T2-PD	0.27

In order to have an idea about the magnitude of the temperature rise due to RF system we will use the result that has been presented in Chapter 5. That is, we can expect the maximum theoretical increase in temperature to be at most double of what has been calculated for only the gradient fields. So, we can find the maximum theoretical temperature rise expectation by multiplying the figures of Table 4 by 2. In Table 5 the maximum theoretical temperature rise values are presented.

Table 5
Maximum theoretical increase in temperature
expected for each protocol.

Name of the MRI protocol	Calculated temperature rise (^{0}C)
SE1 T1	0.72
SE2 T1	0.56
FSE T2	0.24
GE T2-PD	0.54

Nature of the eddy current is to oppose the changes in the magnetic filed. Namely if there is a decrease in the magnetic field in one direction, eddy current is induced in order to increase the field in that direction. This feature of the eddy current results in no current path but the joule heating through the resistance of the conductor. After the joule heating, the thermal energy will be transferred to the neighbouring tissues. So, in our case the surrounding tissues of the implant material will face heating due to the MRI exam conditions. The amount of temperature rise can be calculated as presented above.

4. METHODS

As discussed in Chapter 3 energy will be transferred on metal implants in the form of eddy currents. The path which these currents are dissipated can be modelled as in figure 6. Our electrical circuit model has two resistance connected in parallel to each other, one being the resistance of the implant material and the other being the resistance of the surrounding tissue.

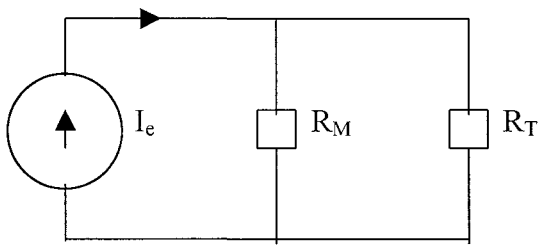

Figure 6. Modelling of the dissipation of the eddy currents through the metal and tissue combination. Where $R_M << R_T$.

The resistance of the tissue is much higher than the resistance of the metal therefore the current will flow mostly through the metal. Also, the nature of the eddy currents implies that the induced current is normally being dissipated through the resistance of the conductor. Based on these facts we made the assumption that the heating of the surrounding tissue are basically due to the heat transfer from the metal. We can safely assume no heating effect through the tissue due to current flow on the tissue, since the MRI operates under the standard settings.

In Chapter 3 we showed that magnetic field change is due to either RF or Gradient or both. To separate the effect of the RF system we have performed some experiments with the RF coils and some without the RF coils.

In this thesis, we have tried to determine the amount of temperature rise of the surrounding tissues for various MRI protocols that are commonly used for orthopaedic cases. We are aiming to differentiate the MRI protocols with respect to the amount of temperature rise that they can cause when the patient carries a metal implant. The amount of temperature

rise is important because of the fact that over 39 ^{0}C the proteins start to denaturate and if the high temperature condition persists damages like local tissue necrosis is possible.

The monitoring of the heating effects is important. We need to monitor any temperature change during the MRI acquisition on the human body, with a metal implant. So, for our work we need the closest environment to the human body. It is not feasible to perform experiments on live tissue because of the difficulty to maintain controlled experimental set-up for long periods. Organic tissue degrades rapidly in the case of excised tissue. Therefore, we need to perform our experiment on a phantom that simulates the tissue behaviour under MRI. The first step is the phantom formation. Since the polyacrylamide gel has close electrical, electromagnetic and thermal properties to the human tissue, it has been used in our experiments to represent human tissue [10,11].

In order for a phantom material to be an effective and convenient one, three different levels of equivalence between the phantom material and the corresponding tissue should be identified for our purposes, namely:

a) Equivalence for the overall electrical performance of the application,

b) Equivalence for the internal electromagnetic power deposition,

c) Equivalence for the internal temperature distribution.

For the electrical and electromagnetic equivalence the phantom material is required to have electrical and electromagnetic permittivity equal to those of the tissues to be simulated. Also for the thermal equivalence, the material should have thermal capacity and conductivity equal to those of the tissues.

The availability of a material having both the electrical and thermal properties corresponding to those of the materials to be simulated permits in principle the performance of an experiment where the temperature is the actual goal of the apparatus. But, on the other hand a very hard task is the reproduction of more complex features of the biological tissues, such as various relaxation mechanisms, nonlinearity and some of the control mechanisms such as blood flow.

For our research, the most appropriate phantom material is polyacrylamide, which has been also used in one of the recent studies [10]. The polyacrylamide gel has close enough thermal and electromagnetic properties to those of living tissues so that it is very effective and

convenient to use this material as a phantom. In Table 6 a brief comparison of phantom and tissue characteristics are presented. As it can be seen from the table, the polyacrylamide gel phantom has close thermal conductivity, specific heat and density values to the human tissue. Similarity in these parameters gives us idea about how close this phantom may represent human body.

Table 6
Comparison of Phantom-Tissue Characteristics

Characte-ristic	**Phantom**	**Living Muscle**	**Excised Muscle**	**Living Skin**	**Excised Skin**	**Living Brain**	**Excised Brain**
Thermal Conductivity (mW/cm. ^{0}C)	4.08	6.42	4.4	4.42	2.5	8.05	5.0
Specific Heat (cal/ ^{0}C.g)	$\approx$ 1	0.83	N.A.	0.90	0.90	0.883	0.883
Density (g / cm^3)	1.03	N.A.	1.07	1.00	1.00	1.05	1.05

The material lends itself for representing high water content tissues such as skin, muscle, and internal organs. The most important properties of the phantom to be considered are the electrical, thermal properties and the stability of the material over a period of time.

The electrical properties of the phantom can be adjusted in order to obtain the desired conductivity and permittivity.

The salt concentration required to obtain a given value of conductivity at a given frequency (shortwave, microwave or RF range) and temperature can be determined from the graphs of conductivity. Reducing the Ammonium Persulphate results in lower conductivity. The frequency dependence is very limited, typically for an increase in the frequency from 13.6

MHz to 40.7 MHz the increase in the conductivity is less than 10%. For our chemical composition and the frequency range the permittivity value was $0.01(\Omega.m)^{-1}$.

The power dissipation on the phantom results in temperature changes. The thermal conductivity and permittivity characteristics of some tissues (fat, skin, muscle) are very close to the values of our phantom, whereas the tissues like bone does not have close correlation. Thus, we can easily say that our phantom can represent tissues like muscle, fat and skin.

4.1 The advantages of using Polyacrylamide Gel as Phantom

Polyacrilamide gel, is also useful for our purposes because of its;

- Transparency in the optical range is excellent,
- Mechanical characteristics of the material lets the phantom to be a self- sustaining one, so that after formation, the phantom sustains with minimum or no mechanical support,
- The entire range of parameters concerning the temperature variations can easily be reproduced,
- Ability to cast in liquid form and after polymerisation additional material with different electrical properties.

Another important reason for choosing this gel as a phantom is that it is very stable over a certain time period. Some loss of solvent, especially water, can be experienced due to diffusion from the phantom into the air or any surrounding absorbing medium. This causes some variation in the electrical properties, and obviously, some mechanical shrinkage. Normally, the electrical and mechanical properties of the polyacrylamide gel are guaranteed to persist for several hours, with ordinary exposure to air. If the stability over weeks is required, like our case, the phantom must be encased in an airtight enclosure when it is not used.

In addition to the above properties the material is low cost and readily available for use in medical analyses.

In order to obtain our phantom we had to investigate the chemical properties of the material. The base formula of the gel is essentially constituted by the polymer of acrylamide,

C_3H_3NO, in water, MBA (N-N-Methylene-Bis-Acrylamide, $C_7H_{10}N_2O_2$), TMEDA or TEMED (N-N-N'-N'- Tetra-Methyl-Ethylene-Diamine, $C_6H_{16}N_2$). Also Cupric Chloride (CuCl) and Ammonium per sulphate ((AP), $(NH_4)_2 S_2 O_8$) are present in the formula as polymerisation catalysts and primers. The preparation of the solution has three phases. For the recipe of 600cm^3 solution we have prepared 540cm^3 solution in phase 1 and 60 cm^3 solution in phase 2 and mix them up in phase 3 the detailed preparation is as follows:

Phase 1) 90 gr of Acrylamide, plus 0.6 gr of MBA and 3.0cm^3 of TMEDA are dissolved in water until a total volume of 540 cm^3 is reached. This mixture is mixed in a magnetic stirrer. The amount of salt (CuCl) required for a desired value of electrical conductivity can be decided from, the curves of conductivity for different temperatures at a given frequency. For our case we have poured 0.2124 gr of CuCl into our 540cm^3 solution and this stage took a time of more than 4 hours. What we get at the end of phase 1 was a royal blue solution.

Phase 2) A solution of Amonium Persulphate (AP) in water is prepared. The volume should be prepared is 60 cm^3 and 1.3 percent by weight.

Phase 3) Solutions of phase 1 and phase 2 are mixed together and the polymerisation reaction has begun.

At room temperature, the solutions of phase 1 and phase 2 have been mixed. Within the first 30 seconds, the polymerisation did not start and it was possible to insert the implant material inside of the mixture and also the thermometers have been inserted in to the mixture. Pre-cooling of the solutions increases the available time. At the end of this 30s period we have taken out the magnet from the magnetic stirrer. And within the next 20 seconds the polymerisation has been completed and the temperature of the mixture has risen to almost 50 ^{0}C.

At the end of phase 3, the obtained solution is a transparent royal blue and highly viscous polymer, such that the orthopaedic implant and the alcohol thermometers can support themselves without any mechanical support. The important thing in this third phase was the avoidance of insertion of anything not later than the first 30second period, because of the possibility of leaving any air gap between the inserted material and the gel, because of the viscosity of the polymer.

4.2 Implant Material

As it has been introduced in the Chapter 2, the implant materials are having a broad range according to their types and the areas of application. In the treatment of fractures, metals are the basic part of the materials because of their strength and ductility. It has been reported that some metals can create an electrical potential when bathed with the saline environment of the soft tissues and cause local tissue necrosis, corrosion of the metal, and resultant loosening of the implants. Which in the end is causing difficulty in the internal fixation of the fractures [6]. To overcome this problem, metals with the lowest electrolytic coefficient have been evaluated and tested [6]. As a result, currently used metal implants became a standard for different internal fixation alternatives [6]. Most commonly used types are 316L stainless steel (composed of iron, chromium, and nickel), titanium aluminium vanadium alloys, or commercially pure titanium (titanium and oxygen).

The material that we have used in our studies is made up of stainless steel and it is called 316L Stainless Steel. This material is chosen because it is the material of preference on the 75% of the fixation procedures [4].

The shape of the implant is a cylinder, which has a radius of 4mm and height of 128 mm. The resistivity, ρ, of the implant material is 6.25×10^{-8} Ω/m. and the permittivity, σ, of the material is 1.6×10^{7} $(\Omega.m)^{-1}$. The mass of the implant is 45 gr.

4.3 MRI Protocols used in the Experiments

The experiments were performed with a 1.5T MRI system. In our studies we have selected two different T1-weighted Spin Echo sequences, one T2-weighted Fast Spin Echo sequence and one Proton Density-T2 weighted Gradient Echo sequence as described in Table 7. For each sequence, we have performed four different measurements. Three measurements were made for the coronal, sagittal and axial image acquisitions. This is done in order to see the effect of each gradient coil. The fourth measurement of each sequence was done when the phantom was not inside the RF coil. This is to see the contribution of RF system to the temperature rise. Common parameters in the experiments were as follows:

Field of view (FOV):	16x16 cm
Number of slices:	10
Slice Thickness:	5 mm
Image matrix:	192x256
Orientation:	Parallel to implant

While choosing our protocols we have tried to select the sequences that are common for imaging the regions that are most likely to contain an orthopaedic implant material. Namely we have tried to select the common sequences for knee, extremities and pelvic region. These MRI sequences are mostly T1 weighted Spin Echo sequences and T2 weighted Fast Spin Echo sequences. Also, sometimes Proton Density and T2 weighted Gradient Echo sequences are being used by the radiologists for imaging these areas of the body.

Table 7
MRI protocols for the Experiments

Protocol Name	**TR (ms)**	**TE (ms)**	**Flip Angle**	**Bandwidth (MHz)**	**Scan Time (s)**	**No of Excitations**
Spin Echo1 **(T1)**	300	20	90^0	15,6	311	4
Spin Echo2 **(T1)**	300	20	90^0	15,6	236	3
Fast Spin Echo1 **(T2)**	2000	105	90^0	15,0	100	4
Gradient Echo**(T2-PD)**	560	11 / 60	60^0	15,6 / 12,5	218	2

4.4 Set-up and the Experiments

The phantom in the beaker, as represented in Figure 7, with the alcohol thermometers inserted in, is put inside the knee coil, and sent back the magnet via the sliding bed of the system. Care has been taken not to move the assembly and the temperature readouts were performed from the very back of the magnet for each protocol. A photo of the phantom inside the knee coil is given in Figure 8.

MR protocols are as summarised in the Table 6.

All MR images are saved in a magneto-optical disk cartridge.

For each MR protocol, the phantom is being scanned and the thermometer readouts were written down.

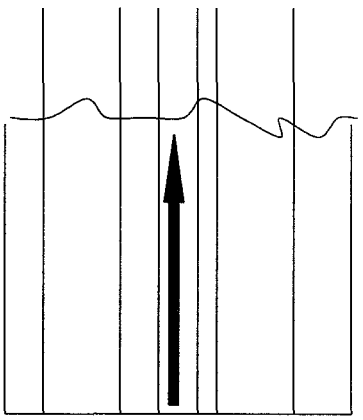

Figure 7. An illustration of the Phantom inside the baker. The straight lines are representing the thermometers, and the block arrow represents the implant material.

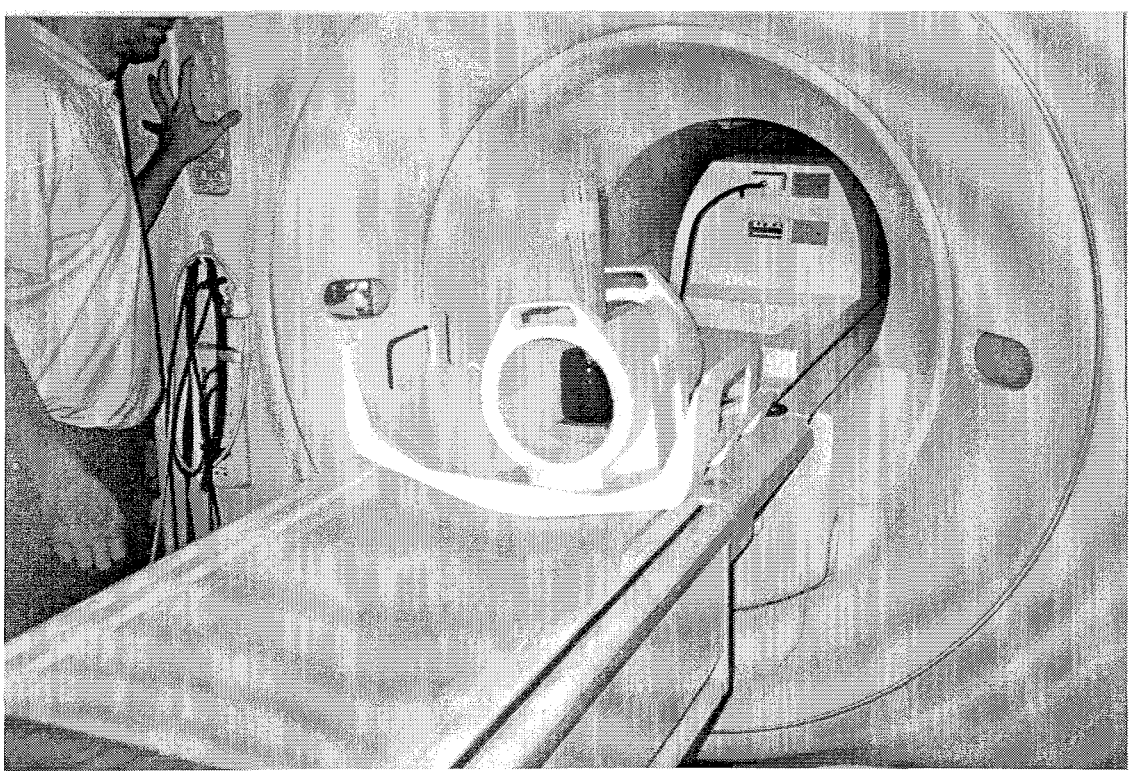

Figure 8. A photo of the Phantom inside the Knee coil of the MRI equipment.

4.5 Experimental Procedure

Temperature measurements were performed using 6 alcohol thermometers in the phantom as illustrated in Figure 7. Alcohol thermometer was selected, since thermocouples, thermistors and mercury thermometers are not suitable to be used in MR environment. The scale of our alcohol thermometers were 0.5 ^{0}C apart. The temperature resolution could not be better than 0.25 ^{0}C. This was acceptable since the temperature rise that would be critical is in the order of 4 ^{0}C and can be measured with these thermometers.

One of the recent studies [10] was based on the relation between the temperature change and the intensity change during different MRI sequences. Temperature resolution and sensitivity for the most common protocols were to be calculated using the phantom experiment results. For our case because of the deflection property of our ferromagnetic implant, to obtain the relation between temperature and intensity is difficult. The deflection due to the metal is affecting the all field of view and the intensity values that have been read out are very diversified from each other.

As it has been stated in the section 3.4 there is a temperature rise expected from the alternating magnetic field upon the metal implant. The cause of the alternating magnetic field on the metal is the gradients of the MRI system. As it has been indicated previously we are assuming no displacement currents on the gel. Also another major contribution to the temperature rise comes from the RF field.

For each predefined MRI sequence we have repeated the same sequence three times with phantom inside the knee coil and one time when the calibration phantom of the equipment were being scanned and our phantom was at the other side of the magnet bore and not inside of the coil. In the first three measurements, we have taken three different combinations of readout, phase and frequency directions. Namely, we have scanned the axial, saggital and coronal images of the phantom. These three directions were repeated because for each direction three gradients were affecting the magnetic field upon the metal from different angles. Certainly, the aim of scanning the phantom without the RF coil has the purpose of showing the difference arising from the RF system. Also when the phantom is at a far distance from the scanning centre we can expect a greater gradient effect. Since it was impossible with

the equipment to connect another coil to our phantom, we could not try the case of scanning a calibration phantom and putting our phantom at a far distance inside another coil.

Design of our phantom was so that, the cylindrical implant material is inserted in the centre of symmetry of the beaker and six different alcohol thermometers were inserted at two symmetrical sides of the implant at equal distances from their symmetric couples. The distance of each thermometer tip from the implant was 0mm (i.e. touching the implant), 6mm and 14mm. If we wish to express the distances from the centre of the metal the distances would be 4mm, 10mm, and 18 mm respectively.

So what we have done is to scan the phantom and measure the amount of temperature rise on the thermometers. The temperature of the MRI room was in the range of 18 - 20 ^{0}C. Because of the cooling system inside of the magnet of the MRI unit, the temperature of the inside of the magnet was 16 ^{0}C. So the initial temperature for our experiment were 16^{0}C.

After obtaining our temperature distribution through the distance, we compared the temperature measurements with the calculated temperature values.

We followed the following steps for each protocol:

- We have put our phantom inside the knee coil and applied the sequence that has been decided previously. Same sequence has been applied three times while the phantom was inside the coil and one time when the phantom was not inside the coil and the water phantom of the equipment were being scanned.
- After each sequence (measurement) we took care of reading the temperatures of the thermometers immediately after the protocol finishes. Since the polyacrylamide gel that we have used in our phantom is homogenous, the distribution of temperature will be uniform at all points of the phantom after a certain time.
- Before starting of the next sequence, we have waited for five minutes for the phantom to cool down for the initial temperature, which is 16^{0}C.

5. EXPERIMENTAL RESULTS AND CONCLUSION

We have used four different MRI protocols as represented in Table7, and for each protocol we have made four different measurements, as mentioned previously in Chapter 4. Also, in Chapter 3 we have calculated the maximum theoretical temperature rises.

In Tables 8, 9, 10 and 11 set of experimental data for T1 weighted SE1 sequence have been presented, respectively. The data in these Tables are the readouts of coronal, sagittal and axial views of the phantom with RF coil and the fourth one is without the RF coil. The reason for changing the readout direction is to see the effect of changing the slice selection and readout direction. Certainly, the aim of scanning without the RF coil is to see the effect due to RF system. The maximum theoretical temperature rise for this protocol was 0.72 ^{0}C, as it has been presented in Table 5.

Table 8
Temperature measurements of the Coronal T1 Weighted
Spin Echo1 Sequence.

Thermometer No.	Distance to Implant (mm.)	Initial Temperature (^{0}C)	Final Temperature (^{0}C)	Difference $T_{final} - T_{initial}$ (^{0}C)
1	18	16.0	16.0	0.0
2	10	16.0	16.25	0.25
3	4	16.0	16.5	0.5
4	4	16.0	16.5	0.5
5	10	16.0	16.25	0.25
6	18	16.0	16.0	0.0

Table 9
Temperature measurements of the Saggital T1 Weighted Spin Echo1 Sequence.

Thermometer No.	Distance to Implant (mm.)	Initial Temperature (^{0}C)	Final Temperature (^{0}C)	Difference $T_{final} - T_{initial}$ (^{0}C)
1	18	16.0	16.0	0.0
2	10	16.0	16.25	0.25
3	4	16.0	16.5	0.5
4	4	16.0	16.5	0.5
5	10	16.0	16.25	0.25
6	18	16.0	16.0	0.0

Table 10
Temperature measurements of the Axial T1 Weighted Spin Echo1 Sequence.

Thermometer No.	Distance to Implant (mm.)	Initial Temperature (^{0}C)	Final Temperature (^{0}C)	Difference $T_{final} - T_{initial}$ (^{0}C)
1	18	16.0	16.0	0.0
2	10	16.0	16.25	0.25
3	4	16.0	16.5	0.5
4	4	16.0	16.5	0.5
5	10	16.0	16.25	0.25
6	18	16.0	16.0	0.0

Table 11
Temperature measurements of the T1 Weighted Spin Echo1
Sequence without RF Coil.

Thermometer No.	Distance to Implant (mm.)	Initial Temperature (^{0}C)	Final Temperature (^{0}C)	Difference $T_{final} - T_{initial}$ (^{0}C)
1	18	16.0	16.0	0.0
2	10	16.0	16.25	0.25
3	4	16.0	16.25	0.25
4	4	16.0	16.25	0.25
5	10	16.0	16.25	0.25
6	18	16.0	16.0	0.0

The results of the T1 weighted Spin Echo2 sequence is presented in Tables 12 through 15. The order of the measurements are, again coronal, sagittal and axial views with RF coil and fourth one is without RF coil. Our reasoning for seeing the effects are the same with our reasoning for Spin Echo1 sequence. Major difference between the previous sequence is Number of Excitations and the scan time. The theoretical maximum temperature rise for this protocol was calculated as 0.56 ^{0}C and this value has been presented in Table 5.

Table 12
Temperature measurements of the Coronal T1 Weighted
Spin Echo2 Sequence.

Thermometer No.	Distance to Implant (mm.)	Initial Temperature (^{0}C)	Final Temperature (^{0}C)	Difference $T_{final} - T_{initial}$ (^{0}C)
1	18	16.0	16.0	0.0
2	10	16.0	16.25	0.25
3	4	16.0	16.25	0.25
4	4	16.0	16.25	0.25
5	10	16.0	16.25	0.25
6	18	16.0	16.0	0.0

Table 13
Temperature measurements of the Saggital T1 Weighted
Spin Echo2 Sequence.

Thermometer No.	Distance to Implant (mm.)	Initial Temperature (^{0}C)	Final Temperature (^{0}C)	Difference $T_{final} - T_{initial}$ (^{0}C)
1	18	16.0	16.0	0.0
2	10	16.0	16.25	0.25
3	4	16.0	16.25	0.25
4	4	16.0	16.25	0.25
5	10	16.0	16.25	0.25
6	18	16.0	16.0	0.0

Table 14
Temperature measurements of the Axial T1 Weighted Spin Echo2 Sequence.

Thermometer No.	Distance to Implant (mm.)	Initial Temperature (^{0}C)	Final Temperature (^{0}C)	Difference $T_{final} - T_{initial}$ (^{0}C)
1	18	16.0	16.0	0.0
2	10	16.0	16.25	0.25
3	4	16.0	16.25	0.25
4	4	16.0	16.25	0.25
5	10	16.0	16.25	0.25
6	18	16.0	16.0	0.0

Table 15
. Temperature measurements of the T1 Weighted Spin Echo1 Sequence Without RF coil.

Thermometer No.	Distance to Implant (mm.)	Initial Temperature (^{0}C)	Final Temperature (^{0}C)	Difference $T_{final} - T_{initial}$ (^{0}C)
1	18	16.0	16.0	0.0
2	10	16.0	16.25	0.25
3	4	16.0	16.25	0.25
4	4	16.0	16.25	0.25
5	10	16.0	16.0	0.0
6	18	16.0	16.0	0.0

In Tables 16 through 19 the results of the T2 weighted Fast Spin Echo sequence is presented in the same order of the previous two sequences. The basic difference is a higher TR and higher TE values and a very short scan time. Number of Excitations is 4. The theoretical calculated temperature rise for this sequence is 0.24 ^{0}C, as it has been presented in Table 5.

Table 16
Temperature measurements of the Coronal T2 Weighted
Fast Spin Echo Sequence.

Thermometer No.	Distance to Implant (mm.)	Initial Temperature (^{0}C)	Final Temperature (^{0}C)	Difference $T_{final} - T_{initial}$ (^{0}C)
1	18	16.0	16.0	0.0
2	10	16.0	16.0	0.0
3	4	16.0	16.25	0.25
4	4	16.0	16.25	0.25
5	10	16.0	16.0	0.0
6	18	16.0	16.0	0.0

Table 17
Temperature measurements of the Saggital T2 Weighted
Fast Spin Echo Sequence.

Thermometer No.	Distance to Implant (mm.)	Initial Temperature (^{0}C)	Final Temperature (^{0}C)	Difference $T_{final} - T_{initial}$ (^{0}C)
1	18	16.0	16.0	0.0
2	10	16.0	16.0	0.0
3	4	16.0	16.25	0.25
4	4	16.0	16.25	0.25
5	10	16.0	16.0	0.0
6	18	16.0	16.0	0.0

Table 18
Temperature measurements of the Axial T2 Weighted
Fast Spin Echo Sequence.

Thermometer No.	Distance to Implant (mm.)	Initial Temperature (^{0}C)	Final Temperature (^{0}C)	Difference $T_{final} - T_{initial}$ (^{0}C)
1	18	16.0	16.0	0.0
2	10	16.0	16.0	0.0
3	4	16.0	16.25	0.25
4	4	16.0	16.25	0.25
5	10	16.0	16.0	0.0
6	18	16.0	16.0	0.0

Table 19
Temperature measurements of the T1 Weighted Fast Spin Echo Sequence Without RF coil.

Thermometer No.	Distance to Implant (mm.)	Initial Temperature (^{0}C)	Final Temperature (^{0}C)	Difference $T_{final} - T_{initial}$ (^{0}C)
1	18	16.0	16.0	0.0
2	10	16.0	16.0	0.0
3	4	16.0	16.25	0.25
4	4	16.0	16.25	0.25
5	10	16.0	16.0	0.0
6	18	16.0	16.0	0.0

In Tables 20 through 23 the results of Gradient Echo sequence have been presented. The four different measurements have been taken for coronal, sagittal and axial views with RF coil and another without the RF coil. The reasoning for the order of measurements is same with the previous three sequences. An important difference of Gradient Echo sequence over the Spin Echo sequences is that, as the name implies Gradient Echo is mostly reversing the gradients and the RF power requirement is therefore less as compared to Spin Echo sequences. Number of Excitations here is 2. Also, there are two different TE values. Theoretical calculated temperature rise for this protocol is 0.54 ^{0}C, as it has been presented in Table 5.

Table 20
Temperature measurements of the Coronal T2-PD Weighted Gradient Echo Sequence.

Thermometer No.	Distance to Implant (mm.)	Initial Temperature (^{0}C)	Final Temperature (^{0}C)	Difference $T_{final} - T_{initial}$ (^{0}C)
1	18	16.0	16.0	0.0
2	10	16.0	16.25	0.25
3	4	16.0	16.5	0.5
4	4	16.0	16.5	0.5
5	10	16.0	16.25	0.25
6	18	16.0	16.0	0.0

Table 21
Temperature measurements of the Saggital T2-PD Weighted Gradient Echo Sequence.

Thermometer No.	Distance to Implant (mm.)	Initial Temperature (^{0}C)	Final Temperature (^{0}C)	Difference $T_{final} - T_{initial}$ (^{0}C)
1	18	16.0	16.0	0.0
2	10	16.0	16.25	0.25
3	4	16.0	16.5	0.5
4	4	16.0	16.5	0.5
5	10	16.0	16.25	0.25
6	18	16.0	16.0	0.0

Table 22
Temperature measurements of the Axial T2-PD Weighted Gradient Echo Sequence.

Thermometer No.	Distance to Implant (mm.)	Initial Temperature (^{0}C)	Final Temperature (^{0}C)	Difference $T_{final} - T_{initial}$ (^{0}C)
1	18	16.0	16.0	0.0
2	10	16.0	16.25	0.25
3	4	16.0	16.5	0.5
4	4	16.0	16.5	0.5
5	10	16.0	16.25	0.25
6	18	16.0	16.0	0.0

Table 23
Temperature measurements of the T2-PD Weighted Gradient Echo Sequence Without RF Coil.

Thermometer No.	Distance to Implant (mm.)	Initial Temperature (^{0}C)	Final Temperature (^{0}C)	Difference $T_{final} - T_{initial}$ (^{0}C)
1	18	16.0	16.0	0.0
2	10	16.0	16.0	0.0
3	4	16.0	16.25	0.25
4	4	16.0	16.25	0.25
5	10	16.0	16.0	0.0
6	18	16.0	16.0	0.0

If we compare the measured experimental results with the theoretical calculated ones, we see that the measurements are slightly less than the calculated ones. This is mostly because

of the heat losses during measurements and reasons like the existence of a heat source inside the magnet for cooling the gradients. Although we have tried to avoid cooling immediately after the scan stop till we read the temperature on the thermometer, it is of course another factor that leads us to measure a little bit less temperature value.

In sum we can conclude that the maximum theoretical or practical temperature rise for a phantom like ours is 0.75 ^{0}C under the imaging conditions that we have used.

6. DISCUSSIONS AND CONCLUSIONS:

During an MRI imaging procedure, the amount of magnetisation and the relaxation constants of the tissues are important factors. Both of these factors are dependent upon the temperature. So, if there is a heating effect, these parameters are also being effected. Although in one of the recent studies [10], the relation between temperature and intensity has been presented, it is impossible for our case to use such a relation because of the deflection property of our metal.

Table 11 of Chapter 5 correspond to the data set of T1 weighted spin echo1 sequence without the usage of RF coil. By comparing the readout values of Table 11 with the previous three we can say that the higher gradient effect arising from higher distance to the scanning centre could not suppress the effect due to RF. This result leads us to be sure that even if we could try the case of putting the phantom at a far distance with another RF coil connected we would get a temperature rise of at most double of what we get now. In Tables 8, 9 and 10 the results of the sequences that have different encoding directions are presented. As it could be seen on these tables the amounts of temperature rise are the same for these three tables. This means that changing the encoding directions of Phase, Frequency and Readout does not effect the amount of temperature rise, that we have measured or our thermometers did not sense the difference in the amount of temperature rise.

There are basically two reasons for temperature rise due to MRI scan, which are the gradient fields and the RF system. For the case of gradient fields, most important factors that cause temperature rise are the duration of the pulse sequence, slew rate of the equipment and the radius of the metal that has been used. As can be observed from Equation 10, the power dissipation is directly proportional to the fourth power of the radius of the implant. The implant material that we have used was the largest possible implant. Also according to the Equations 11 and 12 the duration of the pulse sequences is directly proportional to the energy transferred to the metal. The duration of our sequences is in the range of 100-320 seconds and these values are very typical values. But if more than three or four pulse sequences are going to be applied to the patient there must be some waiting time between the sequences.

Theoretical and experimental investigations concerning heating effects in human tissue during MR scanning have been published previously [12-15]. A mathematical model has been developed and experiments have been performed to determine the heating effects of different types of metallic implants by MR examinations [12-15]. Also, Knepp M et al, in their study has mentioned about a third degree burn in the calves of the patient due to MRI exam [16]. In this study, they have checked for a couple of probable reasons like a malfunction in the MRI equipment, existence of any metal part on the calves or on the RF coil, the SAR limits of the protocols. They have also co-operated with the manufacturer of the equipment to be sure about any effect due to malfunction of the MRI system, and they have noticed that there was not any malfunction of the equipment. And they have also noticed that, there was not any metallic implanted material in the patient body, or the SAR limits were in a very typical range. Also, the duration of the sequences that they have used was a very typical value. Finally, they have concluded that, the reason for such a burn on patient body was very thin left thigh after extensive tumor resection and very muscular calves. This unusual anatomy led to a lack of skin contact between his thighs and to a single small focal skin-to-skin contact zone between his left and right medial calves, which resembled the characteristics of a non-uniform phantom [16]. With this patient, however, the exceptional anatomic characteristics must also be considered. The unusually strong musculature of his calves and the much thinner left thigh led to creation of a particularly large RF current loop that coincided with a lower than normal capacitance between both thighs [16]. There is a mathematical model in which they have represented the situation of the closed loop under MRI in a similar manner to our model. The closed conducting loop occurred in the model has led to a third-degree burn on the focal contact point of the patient's skin.

The results of our experiment showed that there is a temperature rise due to MRI scan applied to an organism which has a metal inserted. On the other hand our results lead us to the result that the maximum possible temperature rise due to MRI scan is around 0.75 ^{0}C. This amount of temperature rise is a tolerable amount of temperature increase for human body. Body temperature is 36.5^{0}C and in the worst case it increases to 37.25 ^{0}C, which is a safe limit for denaturation of the proteins or any local tissue necrosis to occur.

The results of the recent studies show similar findings. In a recent one [13], several types of metallic implant materials had been tested and it is concluded that the heating effect is either very low or very close to zero. Again in another study [15], the classification of the heating effects has been made according to the resistivity and the surface area of the materials used. Heating effect increases with the increased resistivity and stainless steel is among the high resistivity values[15]. A theoretical calculation of the temperature rise on the NiCr Intracranial Depth Electrodes, due to RF system of the MRI has been performed in another study [12], the calculated results were proposing a maximum of 0,107 ^{0}C temperature rise. In this study, the NiCr depth electrodes were chosen since they are normally implanted in to the brain and the brain tissue is more sensitive to the temperature increase other than any tissue [12]. A network analyser has been used in this study to determine the electrode resonant frequency. The measured temperature rise in this study was 0,070 ^{0}C. Electrode resonant frequency measured in this study was not exactly around the proton resonant frequency at 1.5T (64 MHz) and, even if the electrode resonant frequency would be 64 MHz, the absorbed power would be at its peak. And assuming a linear relationship between power absorption and temperature rise it has been calculated that the maximum temperature rise could be 0.4 ^{0}C, which is again a tolerable value [12].

Coming back to our experiment, even though the slew rate parameter of the MRI equipment is one of typical values among current systems, there is some new MRI equipment at the stage of development, which are going to have a slew rate of 125 to 200 T/m/sec. For these new generation MRI system the eddy current phenomenon is one of the major issues, even without the existence of any metallic implant, but because of the affect on the metal ions on the skin. According to Equation 10 the power dissipation on the metal is directly proportional to the square of the slew rate, and a five times increase in the slew rate results in twenty-five times increase in the power dissipation.

Magnitude of the effect of RF is also in a similar range to that of the gradient field. Since the RF system emits RF energy and this energy is in the form of electromagnetic wave there are both energy transfer to the tissues and also the induced eddy currents on the metals. In addition to the cases including implanted metals, like our case, heating effect of RF system is also considered in routine everyday MRI practice as well. However, almost all of the MRI

scanners being used today has a safety limit for RF which is called SAR (Specific Absorption Rate) and thanks to the control of the system by itself, the risk of burning a patient's skin is very low. The SAR limit of a certain study is calculated according to the mass of the patient by using the RF power emission per kilogram of mass parameter of the equipment and if any sequence exceeds this limit the equipment automatically stops scanning.

During the measurements we had difficulties in reading the temperatures on the thermometers and the resolution of our thermometers were very low, but at least we had an idea about the range of the temperature rise. As explained in the earlier sections we could not be able to use more sensitive thermocouples, and may be because of this factor we could not differentiate the effects of each readout direction from each other. But, again, the important temperature rise for us was in a measurable range with our alcohol thermometers.

As a conclusion, for the MRI equipment of today, we can say that the amount of temperature rise is in the limit of 0.75 ^{0}C. And we can further say that application of MRI to the patients who has metallic implant materials inside their body is safe with today's MRI equipment, and we do not expect any local tissue necrosis or protein denaturation. But after the high slew rate equipment became popular, the slew rates of the MRI systems will become five times higher than current values. Since the power dissipation is directly proportional to the square of the slew rate this would mean an increase of twenty-five times in the amount of power dissipation on the metal. That is why we would need to reconsider the conclusions that we have obtained with the current MRI equipment.

REFERENCES:

1. Patton, J.A., *Basics and Instrumentation of MRI,* McGraw Hill, UK, 1992.
2. Rubin, G.D., "Properties of Nitrogen-Implanted Alloys and Comparison Materials," *Surface and Coatings Technology*, Vol. 88, No. 1-3, pp. 132, 1997.
3. Vorwerk, D., F. Redha, "Endosteal Erosion in Association with Stable Uncemented Femoral Components," *Jurnal of Bone and Joint Surgery,* Vol. 72A, No. 7 pp. 1025-1026, 1990.
4. Calay, M., *Statistical Information about the Implant Materials used in Orthopaedics and Traumatologics Department in years 1995 and 1996*, Çapa School of Medicine, İstanbul, 1997.
5. Hayes, D.L., D.R. Holmes, J.E. Gray, "Effect of a 1.5 tesla nuclear magnetic resonance imaging scanner on implanted permanent pacemakers," *J Am Coll Cardiol* Vol. 10, pp. 782-786, 1987.
6. Cooper, L.S., *Hip and Knee Reconstruction*, American Academy of orthopaedic surgeons, McGraw Hill, ILL, USA, 1988.
7. Quint, L.E., *NMR, A perspective on imaging,* General Electric Company, Milwaukee, WI 1982.
8. Bottomley, P.A., C.J. Hardy, R.E. Argersinger, G. Allen-moore, "A review of ^{1}H nuclear magnetic resonance relaxation in pathology: are T1 and T2 diagnostic?," *Med phys* Vol. 14 pp. 25, 1987
9. Partain, C.L., A.E. James, F.D. Rollo, R.R. Price, *Nuclear Magnetic Resonance (NMR) imaging,* McGraw Hill, Philadelphia, 1983.
10. Öztoprak, U., " Temperature Dependence of MRI Sequences," MS. Thesis, Boğaziçi University, 1998.
11. Ho, P.H., C.H. Chen, "Optimisation of Magnetic Resonance Temperature Imaging Sequences," http://www.med.mc.ntu.edu.tw/English/NTU, Bulletin, 1996.

12. Jingxi, Z., L.W. Charles, F.L. Michel, J.B. Eric, B.L. Robert, "Temperature Changes in Nickel-Chromium Intracranial Depth Electrodes during MR scanning," *AJNR*, Vol. 14 pp. 497, 1993.
13. Davis, P.L., L. Crooks, M. Arakawa, R. McRee, L. Kaufman, A.R. Margulis, "Potential hazards in NMR imaging: Heating effects of changing magnetic fields on small metallic implants," *AJR* Vol. 137, pp. 857-860, 1981.
14. Shellock, F.G., D.J. Schaefer, J.V. Crues, "Exposure to a 1.5-T static magnetic field does not alter body and skin temperature in man" *Magn Reson Med*, Vol 11, pp. 371-375, 1989.
15. Buchill, R., P. Boesinger, D. Meier, "Heating effects of metallic implants by MRI examinations" *Magn Reson Med, Vol* 7, pp. 255-261, 1988.
16. Knepp, M., M. Essing, J. Debus, H.J. Zabel, K.G. Van, "Unusual burns of the lower extremities Caused by a closed Conducting Loop in a Patient at MR Imaging," *Radiology,* Vol. 200, pp. 572, 1996.